Supplementary Information (SI) for Chemical Communications.
This journal is © The Royal Society of Chemistry 2025

Electronic Supplementary Information

Stable Zr-based polyoxometalate as a green catalyst for selective oxidation of aniline

Table of Contents

S1 General information

Sodium tungstate dihydrate ($Na_2WO_4 \cdot 2H_2O$) was obtained from Tianjin Kemio Chemical Reagent Co. LTD. Aniline (C_6H_7N), zirconyl chloride octahydrate ($ZrClO_2 \cdot 8H_2O$), tetrahydrofuran (THF), tetramethylammonium chloride ($C_4H_{12}NCl$), sodium carbonate (Na_2CO_3), acetonitrile (CH_3CN), p-fluoro aniline (C_6H_6FN), p-bromoaniline (C_6H_6BrN), p-methoxyaniline (C_7H_9NO), p-chloroaniline (C_6H_6ClN), p-aminotoluene (C_7H_9N), m-toluidine (C_7H_9N), o-toluidine (C_7H_9N), 2-ethylaniline ($C_8H_{11}N$) were purchased from Shanghai Macklin Biochemical Technology Co., LTD. Acetic acid (CH_3COOH), potassium chloride (KCl), phosphoric acid (H_3PO_4), dichloromethane, 1, 2-dichloroethane were purchased from Xilong Scientific Co., Ltd. Ammonium chloride (NH_4Cl), methanol (CH_3OH), sodium acetate (CH_3COONa), acetone, DMF, ethyl alcohol and ethyl acetate was purchased from Shanghai Lingfeng Chemical Reagent Co., LTD. Hydrogen peroxide 30% aqueous solution was purchased from Shanghai Wokai Biotechnology Co., Ltd. All chemicals were of analytical grade and used as received without further purification.

FT-IR spectra were measured by using a Nicolet IS10 FT-IR spectrometer in the 450-4000 cm^{-1} region with KBr pallets. Energy-dispersive X-ray spectroscopy (EDS) measurement was performed on a Regulus8100 scanning electron microscope. Powder X-ray diffraction (PXRD) patterns were recorded on the Rigaku MiniFlex and Rigaku Uitima IV with Cu Kα radiation (λ = 1.54056 Å) in the 2θ range of 5−55°, respectively. Thermogravimetric analysis (TGA) was carried out under N_2 atmosphere from 32 °C to 1000 °C with a heating rate of 10 °C/min on the Netzsch TG 209 F3 Tarsus analyzer. The solid-state diffuse reflectance absorption spectra were recorded on a 2600 UV/vis spectrophotometer with an integrating sphere attachment and BaSO4 as reference. The liquid absorption spectroscopy was recorded on a 759 UV/vis spectrometer using a quartz cuvette with a 1 cm long optical pathway. XPS spectra were measured on a Thermo Scientific ESCALAB Xi+ X-ray photoelectron spectrometer.

S2 Preparation of compound

S2.1 Synthesis of $Na_9[\alpha\text{-}PW_9O_{34}]\cdot 7H_2O$ (Na-PW_9)

The **Na-PW_9** was synthesized according to the literature and characterized by FT-IR [S1]. The detailed process is as follows: 120 g $Na_2WO_4\cdot 2H_2O$ (0.26 mol) was dissolved in distilled water (120 mL). Under vigorous stirring, H_3PO_4 (4 mL) and CH_3COOH (22.5 mL) were added to the above solution, respectively. Then, the solution began to turn cloudy and produced a large amount of white precipitate. After stirring for 1 h, the white precipitate was filtered and dried at room temperature to obtain **Na-PW_9**.

S2.2 Synthesis of Compound

0.51 g **Na-PW_9** (0.2 mmol), 0.13 g $ZrOCl_2\cdot 8H_2O$ (0.4 mmol), 0.15 g $(CH_3)_4NCl$ (1.37 mmol), 0.15 g KCl (2 mmol), 0.11 g NH_4Cl (2 mmol), 0.064 g Na_2CO_3 (0.6 mmol) were dissolved in 10 mL of 0.5 mol·L^{-1} NaAc-HAc buffer (pH = 4.5) and were stirred for 1 h. Then, the mixture was sealed in a 20 mL Teflon-lined steel autoclave at 180 ºC for 12 h. After several days, it was cooled to room temperature, and the colorless square block crystals were obtained (Scheme S1). Yield: 0.15 g (29.34% based on **Na-PW_9**). Elemental analyses calcd. for $C_{36}H_{131}N_9P_2W_{18}O_{81}Zr_3$ (%): H, 2.34; C 7.68; N 2.24; Zr, 4.86; P, 1.10; W, 58.76. Found: H, 1.95; C 7.80; N 2.02; Zr, 5.11; P, 1.00; W, 61.72. IR (KBr pellet, cm^{-1}): 3463(vs), 1076 (vs), 1022(vs), 948(vs), 897(vs), 877(vs), 756(vs), 695(vs), 521(vs).

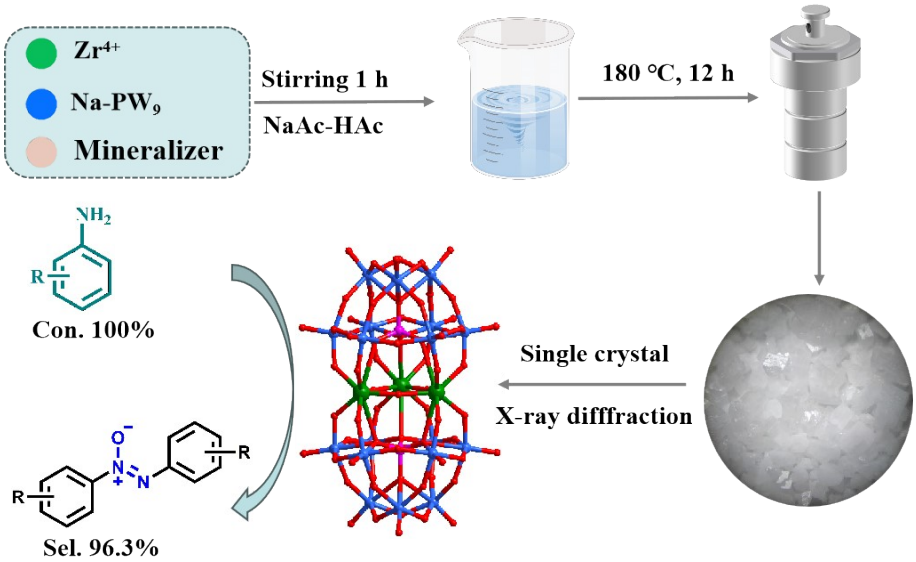

Scheme S1. Synthesis of **Zr-W** via temperature and regulation mechanism of mineralizer for its utilization in thermal-catalytic aniline oxidation to AOB.

S3 Crystallographic data and structure of compound

Crystal X-ray diffraction was made on a hybrid pixel array detector with micro-focus metal jet (λ = 1.3405 Å) at 100 K. The structure was solved with the SHELXT structure solution program using intrinsic phasing and refined with the SHELXL [S2,S3]. Hydrogen atoms were obtained through theoretical hydrogenation, and the number of crystal water was determined through thermogravimetric analysis. The CCDC numbers are 2495653.

Table S1 Crystallographic data of compound **Zr-W**

	Compound **Zr-W**
Empirical formula	$C_6N_{1.5}O_{11.92}P_{0.33}W_3Zr_{0.5}$
Formula weight	891.193
Temperature/K	100.00(10)
Crystal system	Trigonal
Space group	R-3m
a/Å	22.6915(1)
b/Å	22.6915(1)
c/Å	39.2399(2)
α/°	90
β/°	90
γ/°	120
Volume/Å^3	17497.86(14)
Z	36
ρ_{calc}g/cm^3	3.045
μ/mm^{-1}	23.925
F(000)	13262.1
Crystal size/mm^3	0.3 × 0.2 × 0.2
Radiation	micro-focus metaljet (λ = 1.34050 Å)
2Θ range for data collection/°	4.38 to 109.98
Index ranges	$-28 \le h \le 29$, $-28 \le k \le 27$, $-50 \le l \le 50$
Reflections collected	126048
Independent reflections	4006 [R_{int} = 0.0924, R_{sigma} = 0.0193]
Data/restraints/parameters	4006/78/253
Goodness-of-fit on F^2	1.032
Final R indexes [I>=2σ (I)]	R_1 = 0.0347, wR_2 = 0.0860
Final R indexes [all data]	R_1 = 0.0355, wR_2 = 0.0866
Largest diff. peak/hole / e Å^{-3}	2.56/-1.58

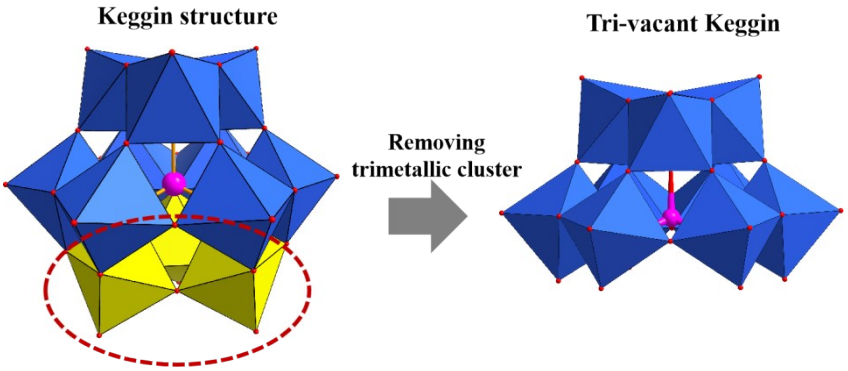

Fig. S1 Formation of tri-vacant Keggin.

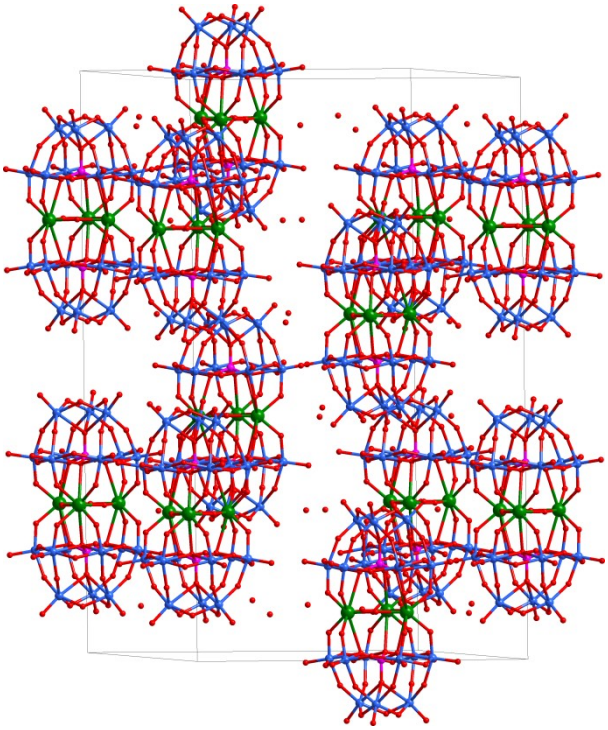

Fig. S2 Packing mode of compound.

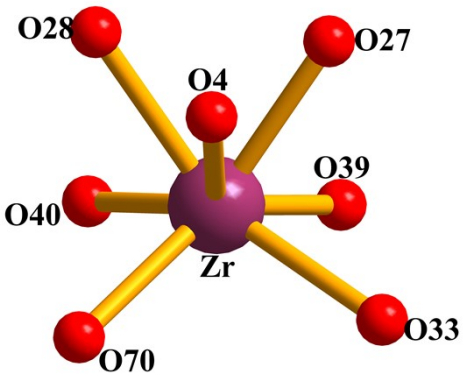

Fig. S3 Coordination environment of Zr ion.

S4 BVS results of W, Zr, P and O atoms

Table S2 BVS results of W, Zr, P and O atoms.

Atom label	BVS value	Atom label	BVS value	Atom label	BVS value
W1	6.28	O3	2.04	O12	1.00
W2	6.23	O4	1.93	O13	1.70
W3	6.22	O5	1.71	O14	2.06
W4	6.22	O6	2.02	O15	2.07
Zr	3.84	O7	2.06	O16	1.96
P1	4.73	O8	1.48	O17	2.01
P2	4.83	O9	1.93	O18	1.94
O1	1.74	O10	1.40	O19	1.75
O2	1.95	O11	1.93		

S5 Characterization data

S5.1 IR spectra

The bonding mode of POM precursor $Na_9[PW_9O_{34}]\cdot 7H_2O$ (**Na-PW$_9$**) and compound **Zr-W** were tested by IR (Fig. S4). The broad absorption peak of **Na-PW$_9$** at 3442 cm^{-1} is assigned to characteristic absorption peak of water molecules. There are obvious characteristic peaks in the range of 1035~1014 cm^{-1}, which is caused by ν(P-O_a) stretching vibration. The characteristic peak at 962 cm^{-1} is attributed to ν(W=O_t) stretching vibration while the peaks at 908 cm^{-1} and in the range of 786~732 cm^{-1} are attributed to ν(W-O-W) stretching vibration. These peaks are consistent with the IR of **Na-PW$_9$** reported in the literature [S1]. The peak of compound at 948 cm^{-1} is attributed to ν(W=Ot) stretching vibration while the peaks at 521 cm^{-1}, 695 cm^{-1}, 756 cm^{-1}, 877 cm^{-1} and 897 cm^{-1} are attributed to ν(W-O-W) stretching vibrations. Meanwhile, the peaks at 1022 cm^{-1} and 1076 cm^{-1} are caused by ν(P-O) stretching vibration, and the peak at 3463 cm^{-1} belongs to ν(O-H) stretching vibration. Compared with the **Na-PW$_9$**, the peaks attributable to the ν(W-O-W) and ν(W=Ot) show obvious shift, which may result from the strong coordination between **Na-PW$_9$** and Zr atoms. Furthermore, compound has an absorption peak at 1485 cm^{-1} attributed to ν(C-H) bending vibration and a peak at 3037 cm^{-1} attributed to ν(C-H) stretching vibration, which is caused by the presence of tetramethylammonium chloride.

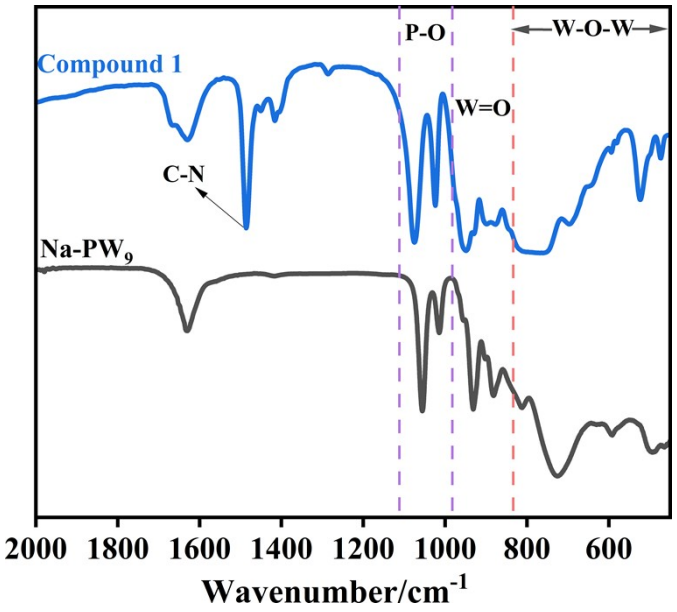

Fig. S4 IR spectra of **Na-PW$_9$** and Compound **Zr-W**.

S5.2 UV spectra

To understand the UV absorption of compound **Zr-W**, the UV spectra were tested. Fig. S5 shows that compound has two peaks at 247 nm and 284 nm, which are attributed to the charge transfer transitions of O→W. Compared with **Na-PW$_9$**, the wavelength corresponding to the peak of maximum absorption has shifted, which might be due to the coordination effect of zirconium.

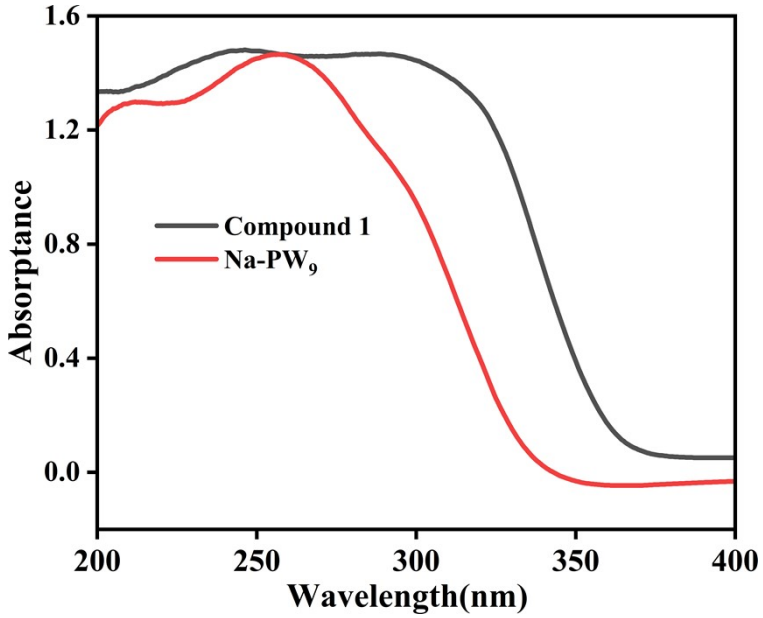

Fig. S5 UV spectra of compound **Zr-W** and **Na-PW$_9$**

S5.3 PXRD patterns

The PXRD pattern of compound is in good consistence with the simulated PXRD pattern from single-crystal X-ray diffraction, indicating good phase purity of compound (Fig. S6).

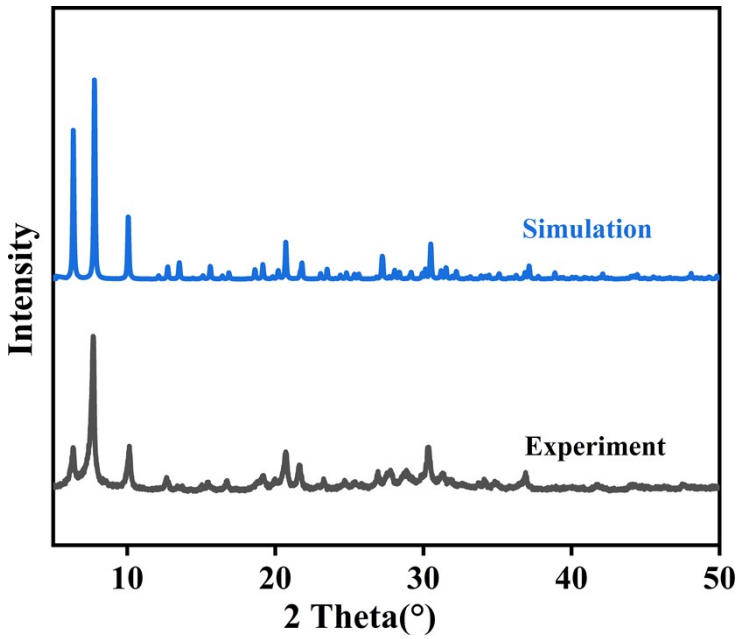

Fig. S6 Simulated and experimental PXRD patterns of compound.

S5.4 TGA curve

To confirm the number of crystal water molecules, TGA curve was tested. As shown in Fig. S7, the TGA curve exhibits two steps of weight loss for compound 1 in the range of 35-800 ℃. The total weight loss rate is 16.0%, which is attributed to the sublimation of crystal water, organic molecules, and phosphorus pentoxide. The first step of weight loss is in the range of 35-150 ℃. The weight loss of this step is about 3.3%, which is attributed to the loss of crystal water. Therefore, it can be concluded that the number of crystal water in compound **Zr-W** is about ten. The second step of weight loss is in the range of 380-800 ℃. The weight loss of this step is about 12.7 %, corresponding to the loss of the organic cations in the form of carbon oxides, water, and nitrogen oxides and the sublimation of P_2O_5 (calcd. 14.85%).

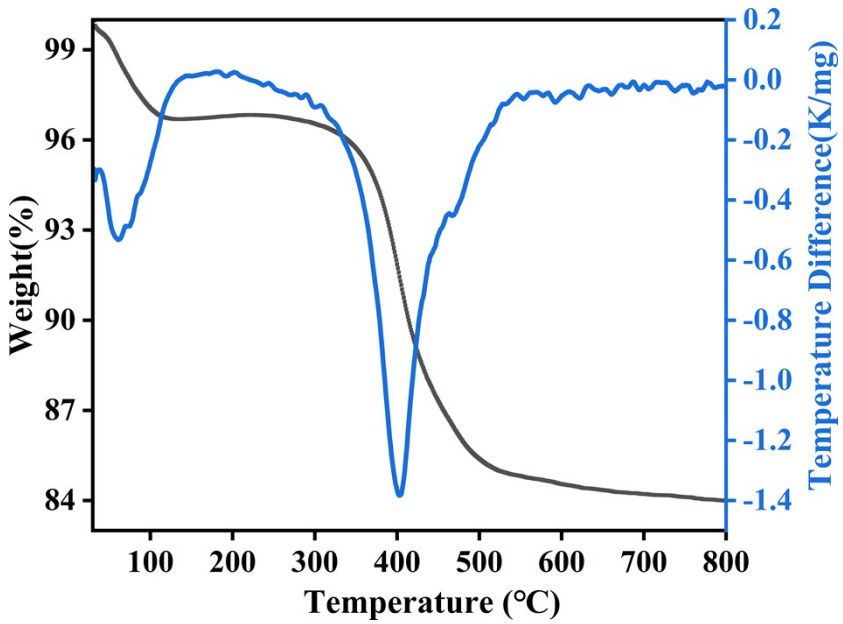

Fig. S7 TGA curve of of compound **Zr-W**.

S5.5 XPS spectra

The valence state and chemical environment of each element in compound **Zr-W** was assessed by XPS. As shown in Fig. S8, compound **Zr-W** contains six elements, which is consistent with the results of X-ray single crystal diffraction analysis. The characteristic peaks at 184.5 eV and 182.0 eV are assigned to Zr 3d, respectively [S4,S5]. The peaks at 37.3 eV and 35.1 eV are assigned to the hexavalent W 4f 5/2 and W 4f 7/2, respectively [S6, S7], and the peak at 133.3 eV is attributed to the electron binding energy of pentavalent P 2p [S8]. The results indicated that the valence states of Zr, W, P were +4, +6, and +5, respectively, in accordance with BVS calculation. The characteristic peak at 286.1 eV is attributed to the C-H bond, while the characteristic peak at the lower binding energy of 284.6 eV is attributed to the C-N bond [S9]. The characteristic peak at the binding energy of 402.2 eV is attributed to the -N+- bond [S10].

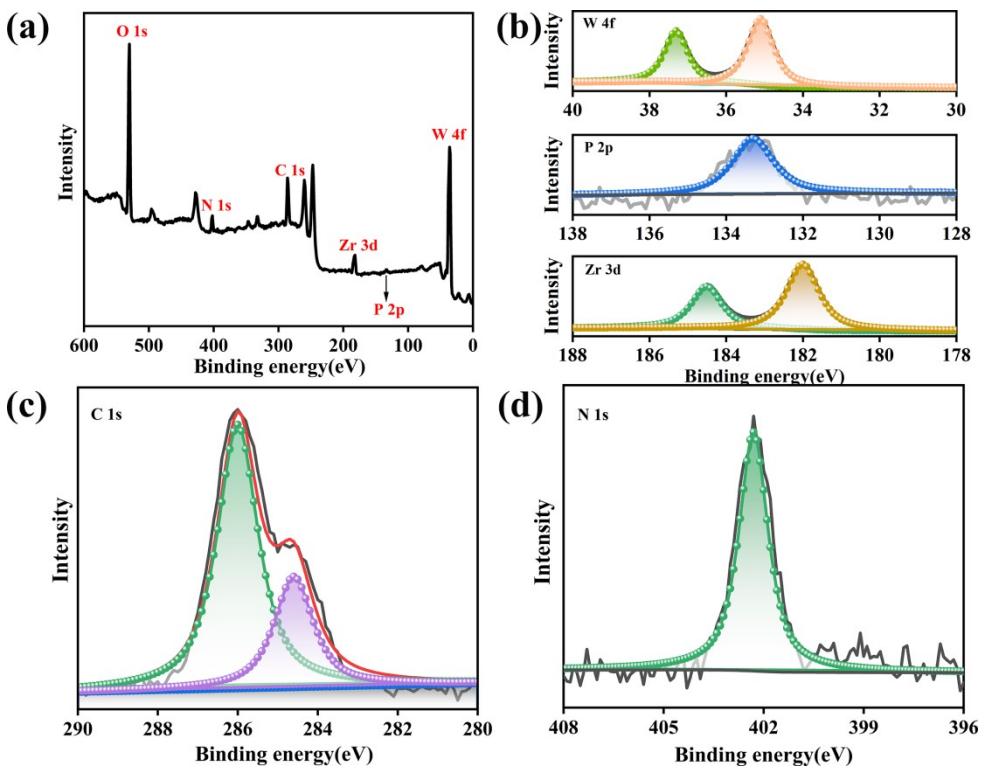

Fig. S8 XPS full-spectra of compound and high resolution XPS of W, P, Zr. C, N.

S5.6 EDS mapping

The distributions of elements were observed by SEM-EDS mapping, indicating the existence of Zr, W and P elements (Fig. 9a-c).

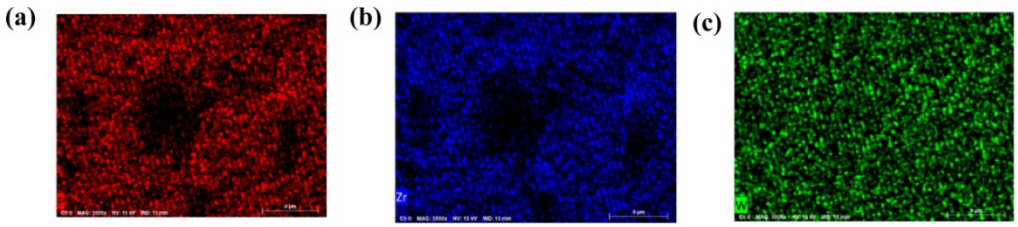

Fig. S9 EDS mapping of Zr, W and P elements on **Zr-W** catalyst.

S6 Catalytic reaction

S6.1 Process of catalytic oxidation of aniline

It is known that the products of the oxidation of aniline are light-sensitive. The reaction was carried out under light-shielding conditions. Aniline (2.0 mmol) is mixed with H_2O (6.0 mL) in a quartz tube, followed by the addition of catalyst (**Zr-W**, x wt% based on aniline) and 30% H_2O_2 aqueous solution. The reaction mixture is then stirred at 700 rpm at designated temperature and time. After the reaction, the obtained dark brown mixture was directly extracted by methanol and for UV spectroscopic and GC-MS (GCTRACE 1300; Agilent 7890B-7000C) analysis. The catalyst was isolated from solution via centrifugation and washed by methanol. And they were employed again to verify the capability for recyclability.

S6.2 Additional figures about catalysis

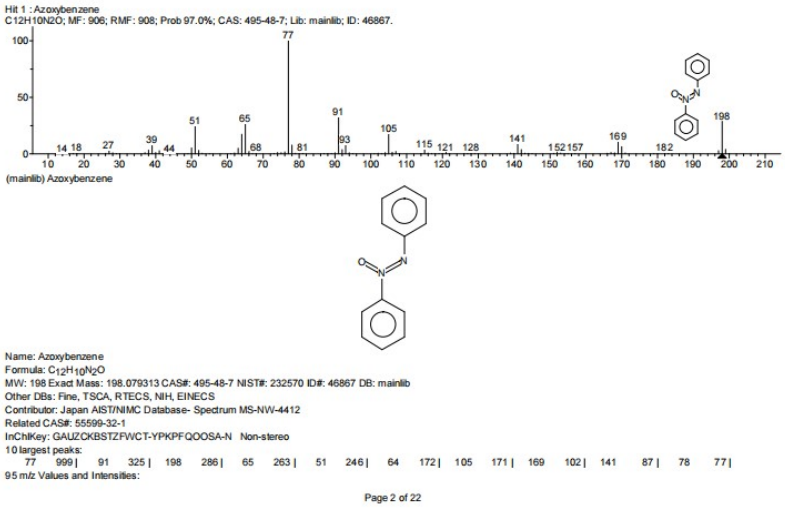

Fig. S10 MS analysis of azoxybenzene

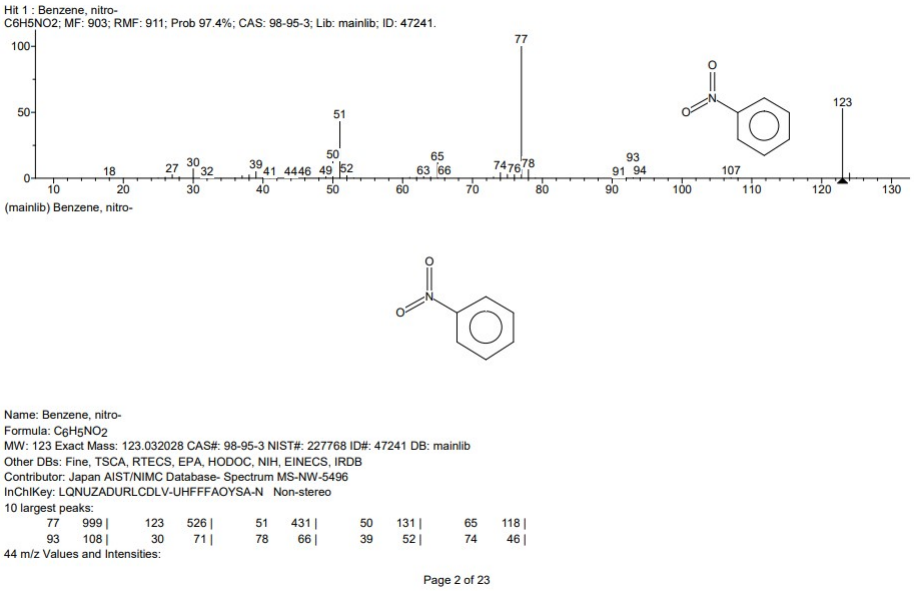

Fig. S11 MS analysis of nitrobenzene

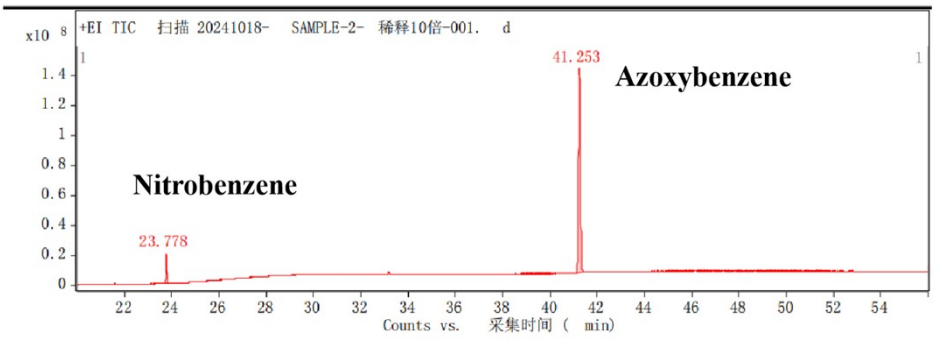

积分峰列表

峰	开始	RT	结束	峰高	面积	峰面积百分比
1	23.723	23.778	23.869	19577323.82	43281614.97	5.27000
2	41.121	41.253	41.438	136145453.9	777959283.93	94.73000

Fig. S12 GC spectra under the optimal catalytic conditions (entry 1, Table 1)

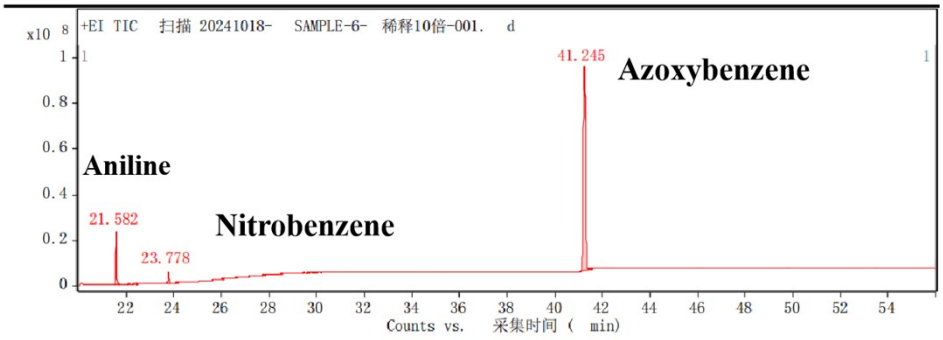

积分峰列表

峰	开始	RT	结束	峰高	面积	峰面积百分比
1	21.529	21.582	21.717	22772013.71	53114327.79	9.28000
2	23.72	23.778	23.858	5092022.57	11727944.51	2.05000
3	41.114	41.245	41.433	89179669.83	507532654.21	88.67000

Fig. S13 GC spectra without catalyst (entry 2, Table 1)

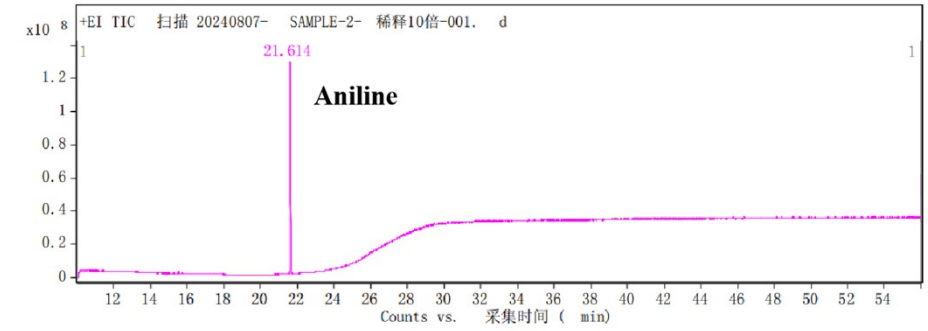

积分峰列表

峰	开始	RT	结束	峰高	面积	峰面积百分比
1	10.123	10.173	10.519	690128.85	10128186.12	3.41000
2	21.56	21.614	21.727	127381608.1	286538180.29	96.59000

Fig. S14 GC spectra without H_2O_2 (entry 3, Table 1)

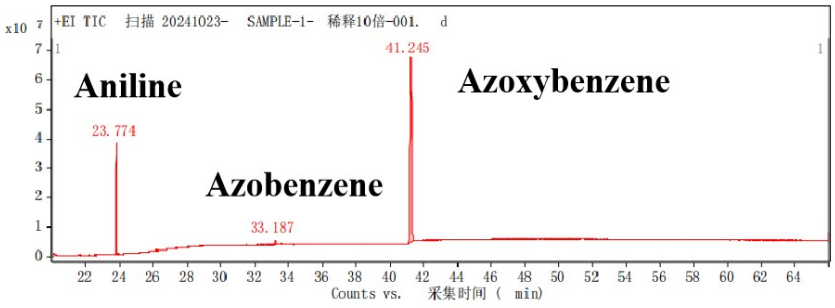

峰	开始	RT	结束	峰高	面积	峰面积百分比
1	23.72	23.774	23.876	37872877.31	82273318.33	19.02000
2	33.119	33.187	33.288	1507603.55	5916795.36	1.37000
3	41.11	41.245	41.394	62714187.64	344345157.84	79.61000

Fig. S15 GC spectra using Na-PW_9 as catalyst (entry 5, Table 1)

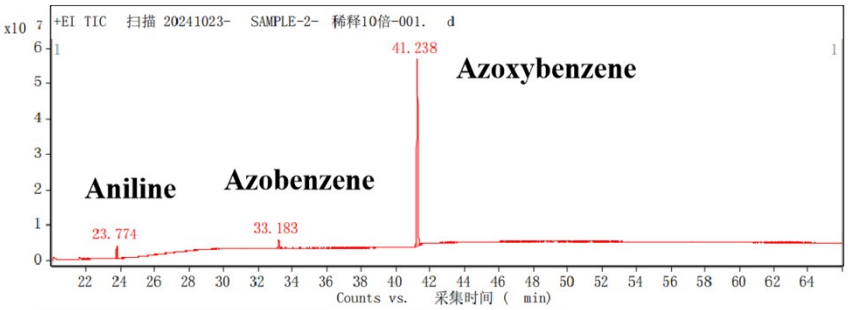

峰	开始	RT	结束	峰高	面积	峰面积百分比
1	23.72	23.774	23.84	3402001.88	7667963.96	2.52000
2	33.117	33.183	33.354	2133943.26	8630634.28	2.84000
3	41.121	41.238	41.411	52602963.47	287775724.68	94.64000

Fig. S16 GC spectra using $ZrOCl_2$ as catalyst (entry 6, Table 1)

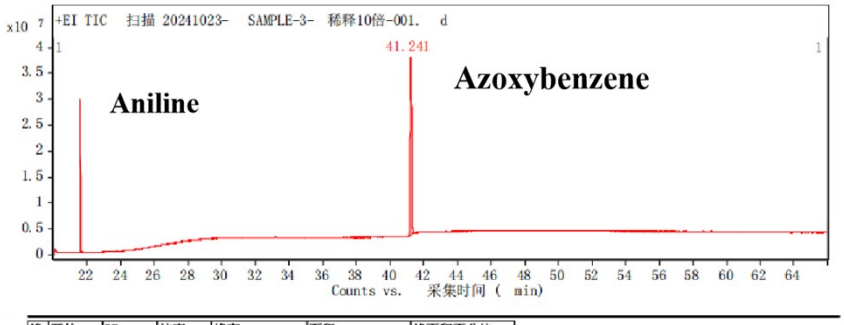

峰	开始	RT	结束	峰高	面积	峰面积百分比
1	21.528	21.579	21.688	29669658.78	64488696.1	25.92000
2	41.114	41.241	41.375	34185701.5	184323834.58	74.08000

Fig. S17 GC spectra using TBHP (entry 4, Table 1)

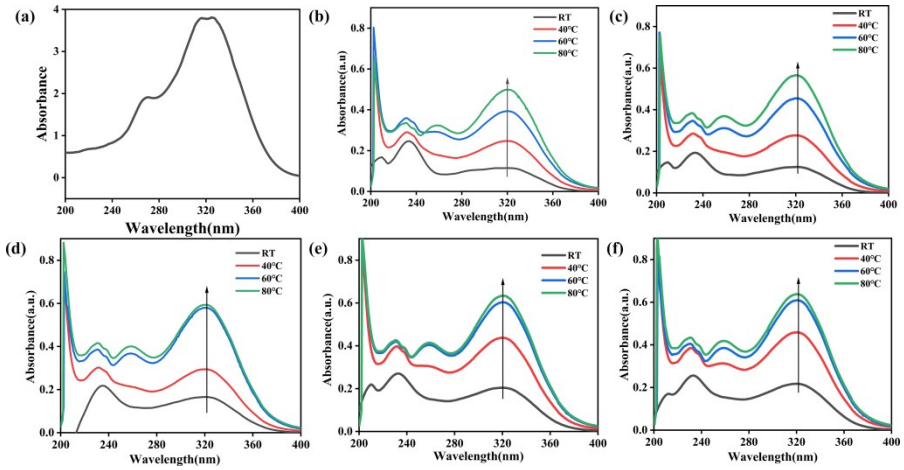

Fig. S18 UV spectra of azoxybenzene and the catalytic product with different reaction times: (a) azoxybenzene; (b) 6 h; (c) 8 h; (d) 10 h; (e) 12 h; (f) 14 h.

The UV spectra of azoxybenzene and the catalytic product are shown in Fig. S18. Compared with azoxybenzene, the catalytic products show similar absorbance peaks,

indicating the formation of azoxybenzene. Besides, under the same reaction time, the intensity of the peak increases with the rise in temperature, indicating that the content of azoxybenzene increases. Likewise, as the reaction time prolongs, the content of azoxybenzene also shows an increasing trend.

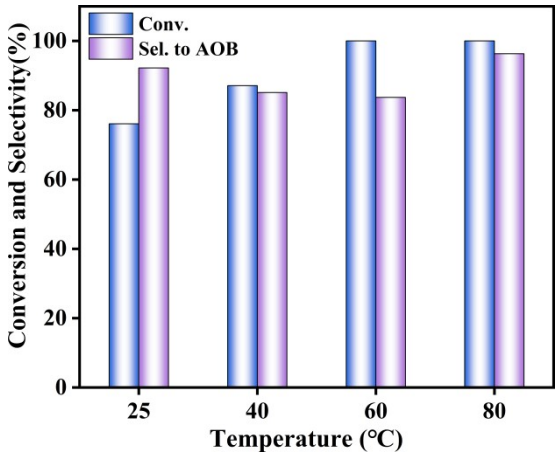

Fig. S19 Conversion of aniline and selectivity to AOB at different reaction temperature

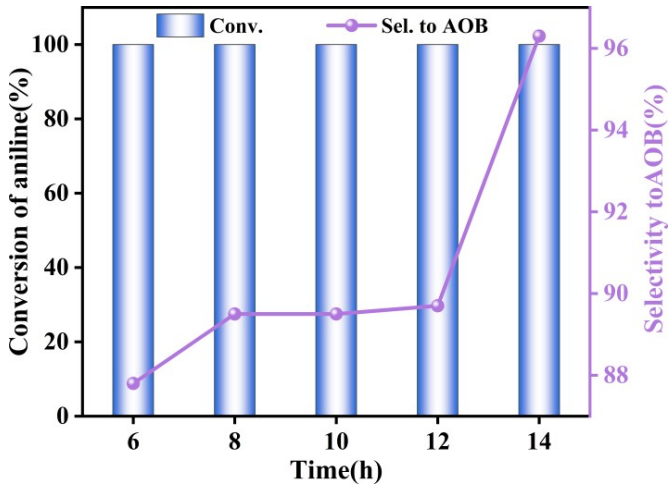

Fig. S20 Conversion of aniline and selectivity to AOB at different reaction times

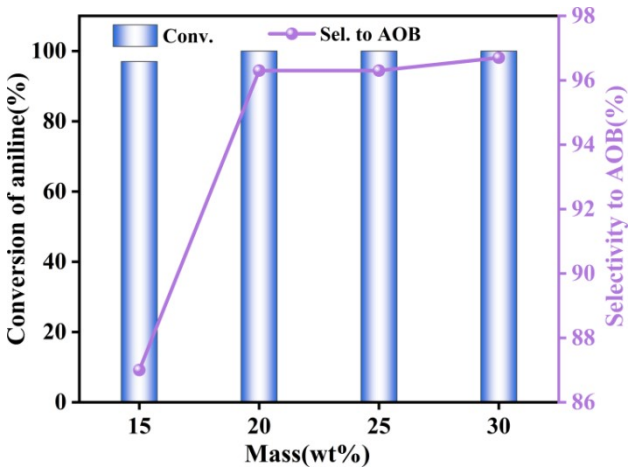

Fig. S21 Conversion of aniline and selectivity to AOB with different dosage of catalyst

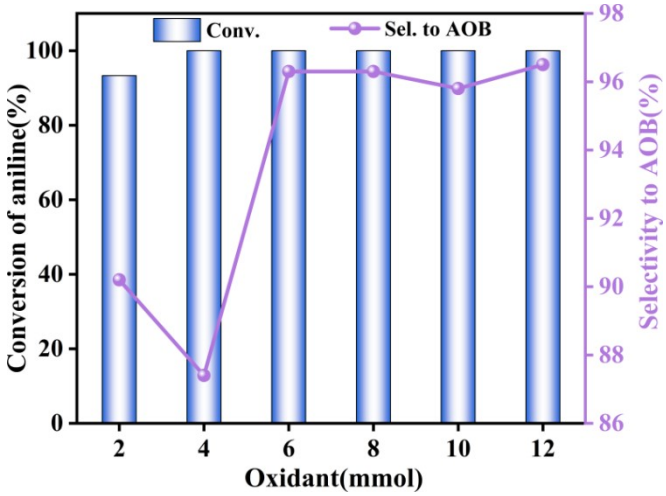

Fig. S22 Conversion of aniline and selectivity to AOB with different dosage of oxidant.

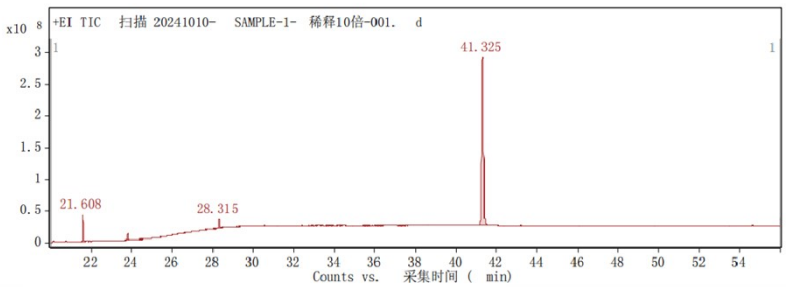

积分峰列表

峰	开始	RT	结束	峰高	面积	峰面积百分比
1	21.553	21.608	21.743	41994694.26	105232021.38	5.95000
2	23.745	23.8	23.873	10253648.63	23749474.43	1.34000
3	28.268	28.315	28.421	13452640.28	38234335.06	2.16000
4	41.176	41.325	41.584	264001544	1600428829.06	90.54000

Fig. S23 GC spectra using DMF as solvent (entry 7, Table 1)

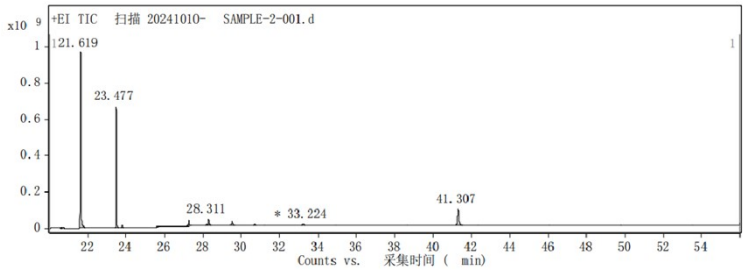

积分峰列表

峰	开始	RT	结束	峰高	面积	峰面积百分比
1	21.545	21.619	21.841	967585480.48	4132792535.86	61.28000
2	23.418	23.477	23.632	669218913.53	1789284631.62	26.53000
3	23.749	23.8	23.855	12046664.09	27086188.58	0.40000
4	25.562	25.631	25.715	2618312.41	6458874.7	0.10000
5	27.224	27.274	27.401	29959240.76	75775160.44	1.12000
6	28.104	28.18	28.253	8006932.16	20318821.6	0.30000
7	28.26	28.311	28.444	30524294.76	86881995.41	1.29000
8	29.437	29.506	29.66	19748933.44	61062690.07	0.91000
9	30.631	30.686	30.78	2227720.41	8258984.59	0.12000
10	33.14	33.224	33.311	3890009.46	15071905.22	0.22000
11	41.173	41.307	41.544	89560375.7	521218343.65	7.73000

Fig. S24 GC spectra using acetone as solvent (entry 8, Table 1)

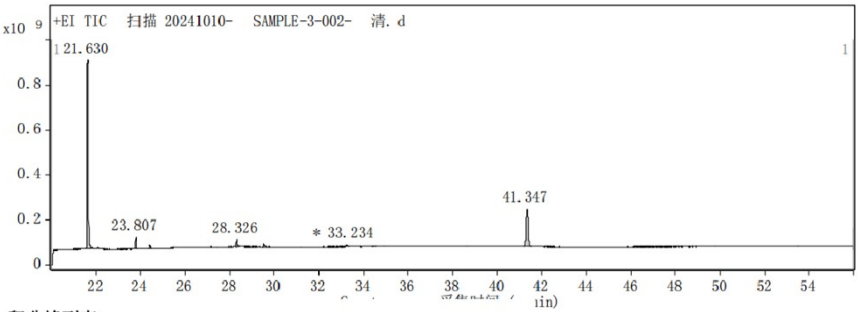

积分峰列表

峰	开始	RT	结束	峰高	面积	峰面积百分比
1	21.556	21.63	21.819	838528142.18	3373108550.62	71.48000
2	23.761	23.807	23.89	47968592.28	111440122.61	2.36000
3	24.377	24.423	24.495	16280988.2	40879940.55	0.87000
4	28.268	28.326	28.468	27516854.3	89546266.69	1.90000
5	29.473	29.52	29.67	11918488.67	45356855.06	0.96000
6	33.154	33.234	33.362	8135003.83	34215475.32	0.73000
7	34.396	34.469	34.622	4335276.74	17704254.15	0.38000
8	41.202	41.347	41.566	161270204.34	1006412931.1	21.33000

Fig. S25 GC spectra using DCM as solvent (entry 9, Table 1)

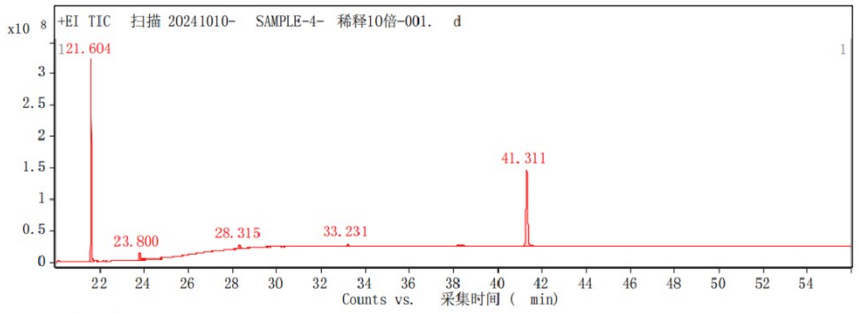

积分峰列表

峰	开始	RT	结束	峰高	面积	峰面积百分比
1	21.546	21.604	21.739	320152182.21	796897567.38	50.79000
2	23.749	23.8	23.895	11075246.14	25756004.19	1.64000
3	28.281	28.315	28.371	4841037.79	11819582.53	0.75000
4	33.161	33.231	33.354	3819587.52	16328478.37	1.04000
5	41.18	41.311	41.62	120156500.59	718344523.13	45.78000

Fig. S26 GC spectra using EtOH as solvent (entry 10, Table 1)

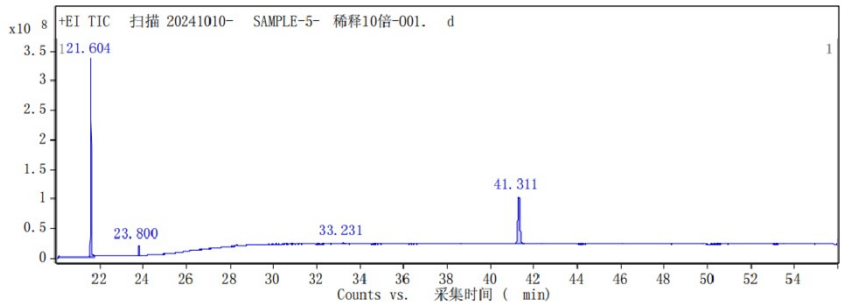

积分峰列表

峰	开始	RT	结束	峰高	面积	峰面积百分比
1	21.546	21.604	21.739	334038883.15	834652065.43	61.95000
2	23.749	23.8	23.876	17210141.99	39207674.31	2.91000
3	33.153	33.231	33.324	3089458.54	11945102.01	0.89000
4	41.176	41.311	41.58	78848584.25	461591839.22	34.26000

Fig. S27 GC spectra using EtOAc as solvent (entry 11, Table 1)

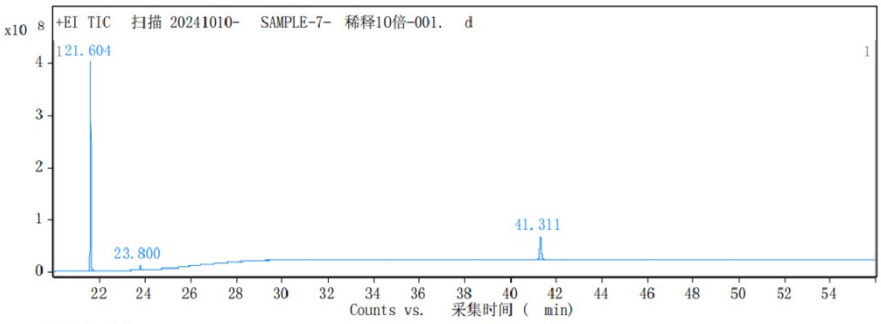

积分峰列表

峰	开始	RT	结束	峰高	面积	峰面积百分比
1	21.542	21.604	21.739	400136604.27	1034960470.49	79.33000
2	23.749	23.8	23.931	6663089.95	16037644.09	1.23000
3	41.18	41.311	41.5	44212837.54	253626181.1	19.44000

Fig. S28 GC spectra using CH_3CN as solvent (entry 12, Table 1)

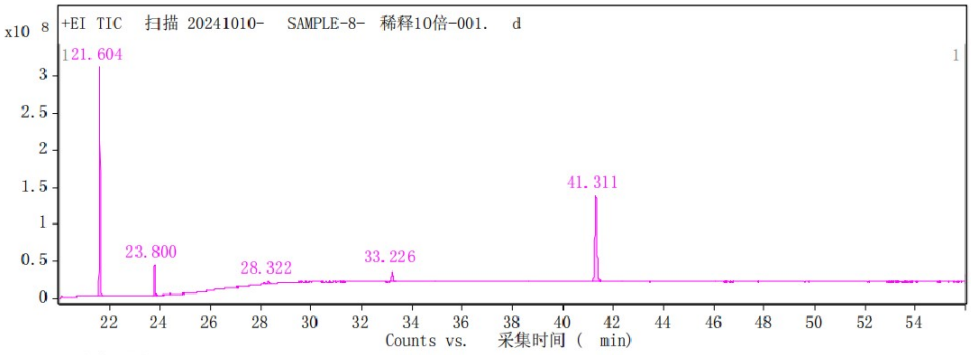

积分峰列表

峰	开始	RT	结束	峰高	面积	峰面积百分比
1	21.542	21.604	21.739	309306631.67	769338952.81	47.49000
2	23.745	23.8	23.913	40428144.27	92208958.14	5.69000
3	28.104	28.155	28.239	2956915.12	8153504.14	0.50000
4	28.281	28.322	28.399	3897064.87	11100297.02	0.69000
5	33.151	33.226	33.398	14141253.71	56594916.09	3.49000
6	41.18	41.311	41.498	114558164.64	682536795.45	42.13000

Fig. S29 GC spectra using 1,2-DCE as solvent (entry 13, Table 1)

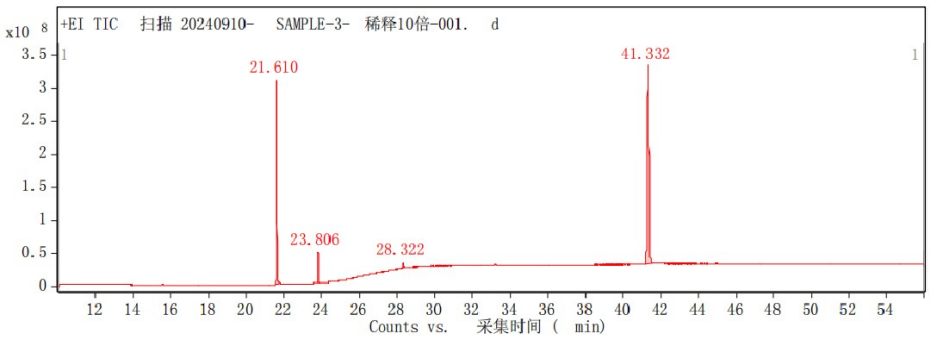

积分峰列表

峰	开始	RT	结束	峰高	面积	峰面积百分比
1	21.549	21.61	21.745	308687915.75	788382278.87	28.83000
2	23.752	23.806	23.912	46684097.9	105250562.51	3.85000
3	28.275	28.322	28.413	9578418.48	28968000.22	1.06000
4	41.197	41.332	41.609	298630427.48	1811724749.35	66.26000

Fig. S30 GC spectra using MeOH as solvent (entry 14, Table 1)

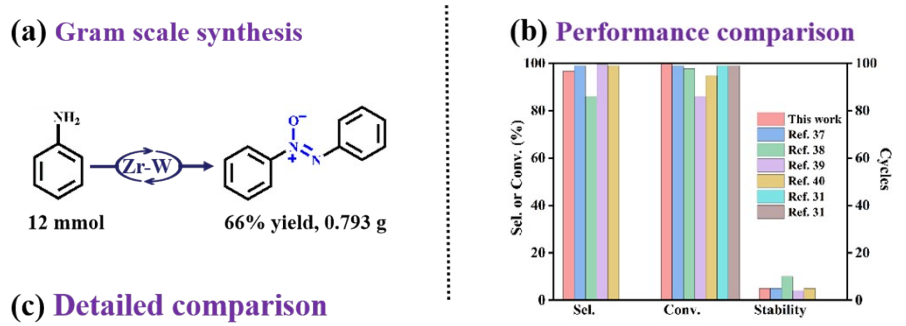

(c) Detailed comparison

Entry	Sel.	Conv.	Stability	Main product	Catalytic method	Catalyst	Ref.
1	96.7%	100%	5 cycles	azoxybenzene	Thermocatalysis	Zr-W	This work
2	99.9%	99.9%	5 cycles	azobenzene	Ultrasound-assisted thermocatalysis	$\{CoMo_6\}$ and additives	37. Sep. Purif. Technol. 2025, 365 132687
3	99%	99%				$\{CoMo_6\}$	
4	86.0%	97.7%	10 cycles	nitrosobenzene	Thermocatalysis	$\{Ce_3(GeW_9)_2\}$	38. Inorg. Chem. Commun. 2023, 154, 110912
5	86.0%	99.4%	4 cycles	azoxybenzene	Thermocatalysis	$\{Ni_6PW_9\}$	39. Chin. Chem. Let. 2024, 35, 108324
6	99%	94.7% (yield)	5 cycles	azobenzene	Thermocatalysis	$\{Rh_4As_4W_{40}\}$ and additives	40. Chem. Commun. 2022, 58, 9902
7	/	99% (yield)	/	azobenzene (CH_3OH)	Thermocatalysis	$\{Mo_6O_{19}\}$ and additives	31. Angew. Chem. Int. Ed. 2021, 60, 6382 –6385
8	/	90% (yield)	/	azoxybenzene (MTBE)			

Fig. S31 (a) Gram scale synthesis. (b,c) Comparison of catalytic performance of different polyoxometalate catalysts as reported.

Table S3 Optimization of the reaction conditions.

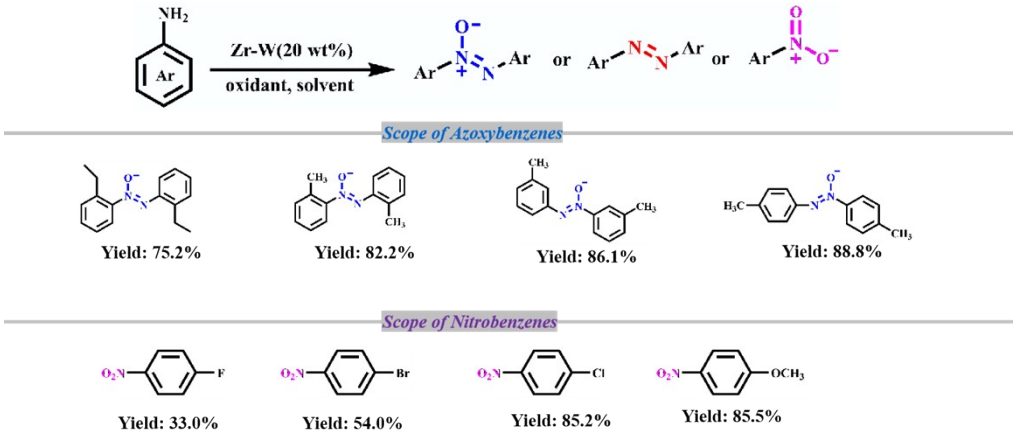

S7 Mechanistic studies

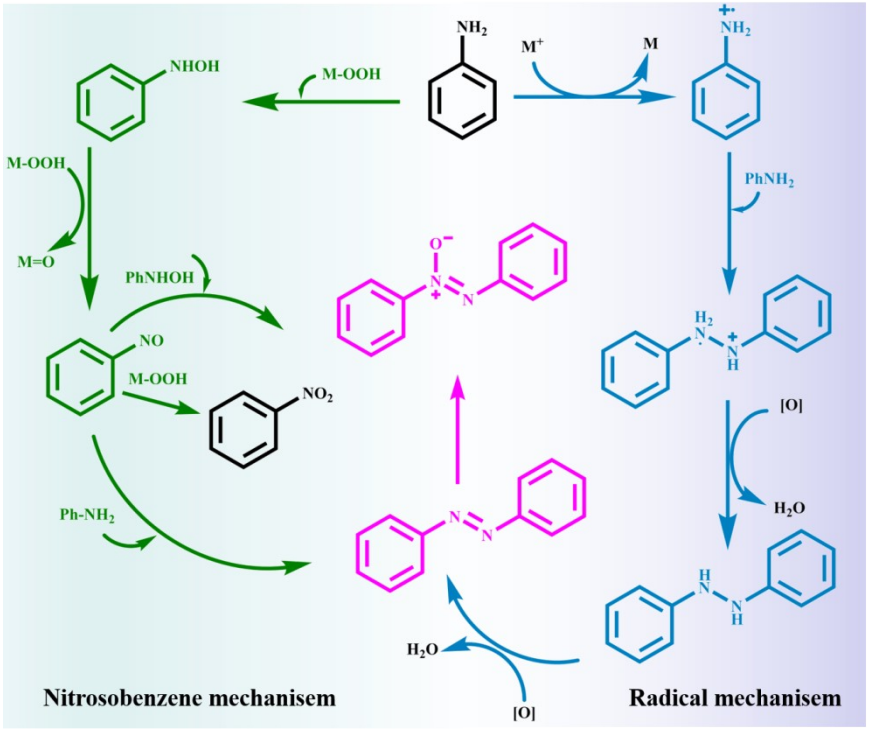

Fig. S32 Schematic diagram of aniline oxidation mechanisms: nitrosobenzene mechanism and radical mechanism.

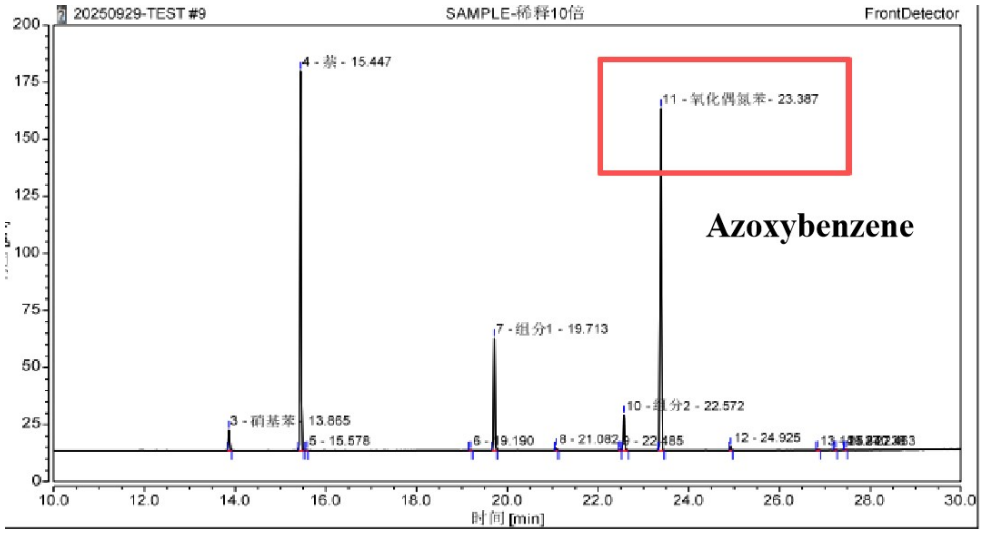

Fig. S33 GC analysis of reaction with BHT.

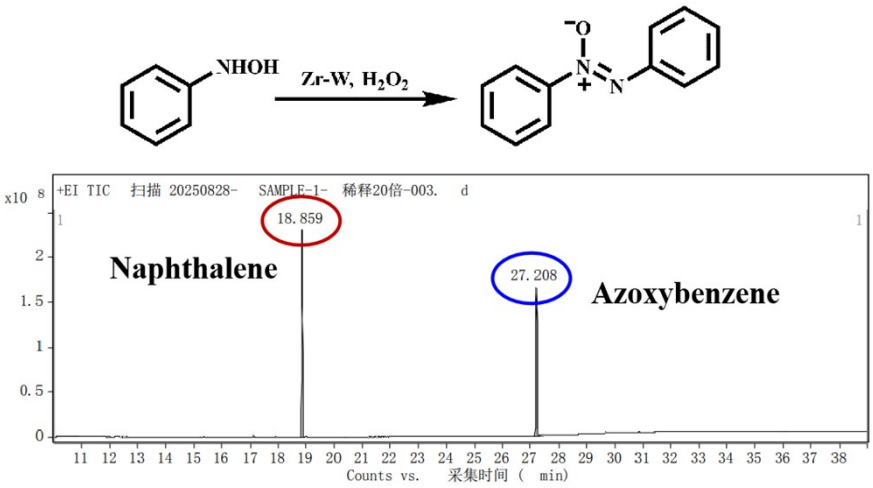

Fig. S34 Reaction process with hydroxyaniline as substrate.

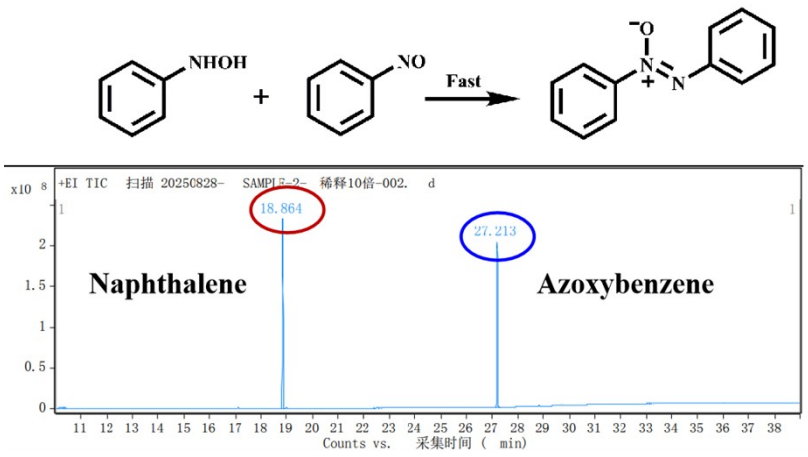

Fig. S35 Reaction process with hydroxyaniline and nitrosobenzene as substrate.

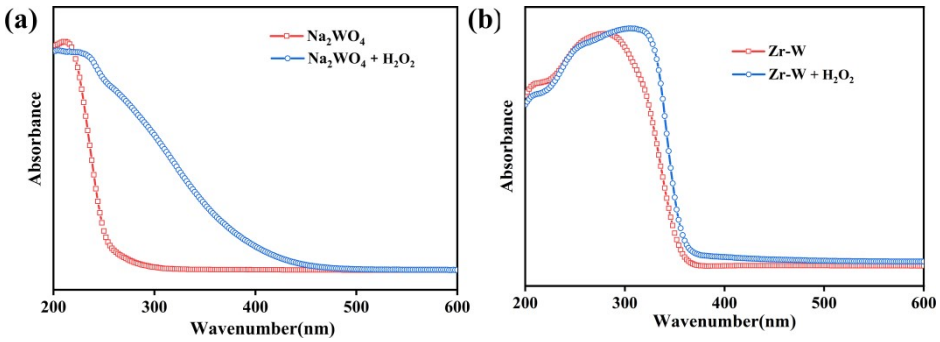

Fig. S36 UV-vis spectra of different samples.

S8 Reference

[S1] P. J. Domaille, G. Hervéa and A. Téazéa, in Inorganic Syntheses, ed. A. P. Ginsberg, Wiley, 1st edn., 1990, **27**, 96-104.

[S2] O.V. Dolomanov, L. J. Bourhis, R.J. Gildea, J.A.K. Howard and H. Puschmann, ***J. Appl. Cryst.***, 2009, **42**, 339-341.

[S3] G.M. Sheldrick, ***Acta Cryst.***, 2015, **A71**, 3-8.

[S4]S. Ardizzone and C. L. Bianchi, ***Appl. Surf. Sci.***, 1999, **152**, 63-69.

[S5] G. Bakradze, L. P. H. Jeurgens and E. J. Mittemeijer, ***J. Phys. Chem. C***, 2011, **115**, 19841-19848.

[S6] Q. Zhu, H. An, T.-Q. Xu, Y. Chen, Y. Wei and H. Sun, ***ACS Sustainable Chem. Eng.***, 2024, **12**, 1655-1665.

[S7] Y. Kamiura, K. Umezawa, Y. Teraoka and A. Yoshigoe, ***Mater. Trans.***, 2016, **57**, 1609-1614.

[S7] M. Lee, S. Kim and D.-H. Ko, ***Appl. Surf. Sci.***, 2018, **443**, 131-137.

[S9] X. Xu, J. Zhang, Z. Zhang, G. Lu, W. Cao, N. Wang, Y. Xia, Q. Feng and S. Qiao, ***Nano-Micro Lett.***, 2024, **16**, 116.

[S10] S.-W. Li, Z. Yang, R.-M. Gao, G. Zhang and J. Zhao, ***Appl. Catal. B: Environ.***, 2018, **221**, 574-583.